Front. Earth Sci. 2021, 15(1): 151–166
https://doi.org/10.1007/s11707-020-0846-9

RESEARCH ARTICLE

Relationship between the Tibetan Plateau–tropical Indian Ocean thermal contrast and the South Asian summer monsoon

Xiaoqing LUO[1,2], Jianjun XU (✉)[1,2], Yu ZHANG[1,2], Kai LI[3]

1 South China Sea Institute of Marine Meteorology, Guangdong Ocean University, Zhanjiang 524088, China
2 College of Ocean and Meteorology, Guangdong Ocean University, Zhanjiang 524088, China
3 Maritime College, Guangdong Ocean University, Zhanjiang 524088, China

Abstract The impact of land–sea thermal contrast on the South Asian summer monsoon (SASM) was investigated by calculating the atmospheric heat sources (AHS) and baroclinic component with ERA5 data for the period 1979–2019. Using diagnostic and statistical methods, it was found that the thermal contrast between the Tibetan Plateau (TP) and the tropical Indian Ocean (TIO) affects the South Asian monsoon circulation through the meridional temperature gradient in the upper troposphere. The seasonal changes of the AHS of the TP and TIO are reversed. In summer, the TP is the strongest at the same latitude whereas the TIO is the weakest, and the thermal contrast is the most obvious. The heat sources of the TP and TIO are located on the north and south side of the strong baroclinic area of the SASM region, respectively, and both of which are dominated by deep convective heating in the upper troposphere. The TP–TIO regional meridional thermal contrast index (*QI*) based on the AHS, and the SASM index (*MI*) based on baroclinicity were found to be strongly positively correlated. In years of abnormally high *QI*, the thermal contrast between the TP and TIO is strong in summer, which warms the upper troposphere over Eurasia and cools it over the TIO. The stronger temperature gradient enhances the baroclinicity in the troposphere, which results in a strengthening of the low-level westerly airflow and the upper-level easterly airflow. The anomalous winds strengthen the South Asian high (SAH), with the warmer center in the upper troposphere, and the enhanced Walker circulation over the equatorial Indian Ocean. Finally, the anomalous circulation leads to much more precipitation over the SASM region. The influence of abnormally low *QI* is almost the opposite.

Received August 5, 2019; accepted October 18, 2020

E-mail: gmuxujj@163.com

Keywords Tibetan Plateau, tropical Indian Ocean, atmosphere heat sources, South Asian summer monsoon, atmosphere baroclinic component

1 Introduction

The South Asian summer monsoon (SASM) is the strongest among the three members of the Asian monsoon system (Wang et al., 2017), and the summer precipitation (June–September, accounting for about 80% of the total annual amount) can affect the lives of about one billion people (Kripalani et al., 2003). The intensity of the SASM, which is affected by land–sea thermal contrasts (Webster et al., 1998; Turner and Annamalai, 2012), can impact on precipitation (Wang et al., 2013; Naveendrakumar et al., 2019). The greater the thermal contrast between Eurasia and the Indian Ocean, the stronger the SASM circulation, and the more monsoon precipitation. Hence, anomalous land–sea thermal contrast may lead to extreme climate events (Roxy et al., 2015).

However, meridional and zonal thermal contrast indices between the land and sea, which are always based on temperature, are not uniform (Dai et al., 2013). Different definitions of land–sea thermal contrast, based on factors such as surface temperature (Fu and Fletcher, 1985; He et al., 2014), mid-tropospheric temperature (Sun et al., 2010), mean tropospheric temperature (Liu and Yanai, 2001), and upper-tropospheric temperature (He et al., 2003), have been used to study monsoon circulation variations. Fu and Fletcher (1985) found that the difference between the surface temperature of the Tibetan Plateau (TP) and the sea surface temperature (SST) of the Pacific equatorial cold tongue is significantly related to SASM precipitation, while Liu and Yanai (2001) identified that the 200–700-hPa mean temperature of Eurasia has a strong

relationship with SASM precipitation. Li and Yanai (1996) found that the 200–500 hPa meridional temperature difference has a strong positive correlation with the intensity of the summer monsoon. Sun et al. (2002) used the surface temperature to establish a comprehensive land–sea thermal index to research the East Asian monsoon circulation, and Chou (2003) used a model to prove that the meridional temperature gradient increases, resulting in a strengthening of the monsoon circulation, when the tropical SST is anomalously cold, or the albedo of Eurasia and the TP decrease or the atmospheric heat source (AHS) increases. However, Dai et al. (2013) used reanalysis data and numerical simulation experiments to show that the land–sea difference in the upper-tropospheric temperature has greater impact on the monsoon. These studies have described the land–sea thermal contrast at different levels of the Asian monsoon region and reached different conclusions. From the thermodynamic equations, it can be seen that the local temperature change is the result of horizontal advection, vertical transportation, and the AHS (also known as non-adiabatic heating). Using the surface temperature between the land and sea cannot explain the deep convective heating of the SASM, and the results might be different at different levels (Sun et al., 2010; Dai et al., 2013). The spring sensible heating over the TP region is likely to affect the distribution of large-scale temperature meridional gradients in the upper troposphere, which can impact the onset and intensity of the Asian monsoon (Li and Yanai, 1996). Therefore, there is a problem in using the temperature to construct sea–land thermal difference indexes to study its relationship with the monsoon. Rather, the AHS difference between Eurasia and the Indian Ocean might be a good indicator to measure the thermal contrast between the land and sea, and some scientists have indeed used the AHS to define land–sea thermal contrast indexes (Zhang et al., 2017).

Fu and Fletcher (1985) defined a zonal thermal contrast index, which has a significant correlation with the SASM index, but there are still some uncertainties among different SASM indices. For instance, AIRI (All Indian Summer Rainfall Index) (Parthasarathy et al., 1992; Sontakke et al., 1993) cannot describe the large-scale monsoon circulation, and WYI (the Webster and Yang index (Webster and Yang, 1992), and MH (monsoon Hadley) index (Goswami et al., 1999) cannot successfully describe the monsoon precipitation. It is complicated using the standardized seasonal variability to define a monsoon index (Li and Zeng, 2002), and yet there are problems with monsoon indexes constructed using convection activities (Wang and Fan, 1999). Because the monsoon is significantly affected by the thermal contrast between the land and sea, atmospheric motion exhibits obvious baroclinic characteristics (Guan, 2000). Previous studies have constructed monsoon indexes with an atmospheric baroclinic component (Guan et al., 1997; Xu and Chan, 2002); for example, Xu and Chan (2002) defined an SASM index that has a significant correlation with WYI and AIRI.

The AHS is the sum of surface sensible heat, precipitation condensation latent heat, and net atmospheric radiation, which can drive large-scale circulation (Yanai et al., 1992). The Asian monsoon region is one of the main regions of the global AHS, and the sea and land distributions of heat sources are quite different (Yanai and Tomita, 1998). The South Asian High (SAH) and the Western North Pacific Subtropical High are located on the west and east of the Asian monsoon AHS region, respectively, and the intensity of the heating center has a significant impact on the formation and strength of the two large-scale systems (Liu et al., 1999). In turn, the SAH is one of the important subsystems of Asian summer monsoon circulation, which can affect the monsoon heating center (Tu et al., 2020). The AHS not only affects the monsoon circulation, but also the water vapor exchange (Zhan and Li, 2008). There have been many studies on the thermal effects of the TP (Yanai and Wu, 2006; Wu et al., 2005; Wang et al., 2008; Wu et al., 2012; Luo et al., 2019; Luo and Xu, 2019; Zhao et al., 2019), but most of them focused on the influence of the plateau's thermal effects on the monsoon circulation independently (Liu et al., 2002; Liu et al., 2012). Zhang et al. (2017) defined a meridional thermal index of the TP and the southern Indian Ocean with the AHS and pointed out that the index is closely related to the onset of the SASM. The TP (75°E–103°E, 28°N–38°N) and the tropical Indian Ocean (TIO; 60°E–100°E, 15°S–5°N) are at the same longitude and are simultaneously affected by the South Asian monsoon (SAM; 40°E–100°E, 0°–20°N) (Fig. 1).

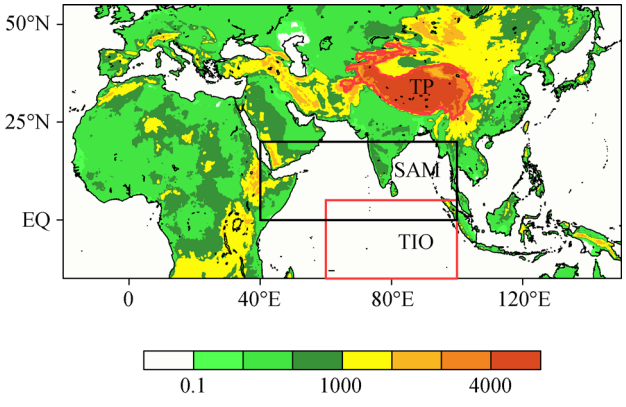

Fig. 1 Study area, showing the topography (shaded; unit: m) of the Tibetan Plateau (TP; 75°E–103°E, 28°N–38°N; altitude≥ 3000 m; bordered in red), the tropical Indian Ocean (TIO; 60°E–100°E, 15°S–5°N; red box) and the South Asian monsoon region (SAM, 40°E–100°E, 0°–20°N; black box).

Important questions, however, remain unanswered. For example, how might we quantitatively characterize the thermal contrast in the TP–TIO region and the SAM

index? What is the relationship between the thermal contrast and the SASM? The physical mechanisms underpinning the effects of different land–sea thermal contrasts on the monsoon circulation also need to be further studied. This paper attempts to establish the mechanism involved in the relationship between the meridional thermal contrast of the TP–TIO region and the monsoon circulation. Section 2 describes the data and methods. Section 3 compares the different TP–TIO thermal contrasts. Section 4 describes the change in the SASM, with Section 5 reporting the relationship between the thermal contrast and the SASM, followed by a summary of the results and some further discussion in Section 6.

2 Data and methods

2.1 Data

To compute the AHS and atmospheric moisture source (AMS), we used ERA5 (period: 1979–2019; resolution: 1° × 1°) monthly data of air temperature, specific humidity, horizontal wind speed, and vertical wind speed at standard pressure levels (1000, 975, 950, 925, 900, 875, 850, 825, 800, 775, 750, 700, 650, 600, 550, 500, 450, 400, 350, 300, 250, 225, 200, 175, 150, 125 and 100 hPa). ERA5 is the fifth generation of the ECMWF (European Centre for Medium-Range Weather Forecasts) global atmospheric reanalysis, from 1950 to the present day. Compared to the 80 km for the ERA-Interim reanalysis data set, ERA5 has a horizontal resolution of 31 km, which performs better in describing temperature, wind, precipitation, weather systems, and so on (Hersbach et al., 2020). The present study also used ERA5 potential height to analyze the SAH in summer and calculate the atmospheric baroclinic component with horizontal wind. In the following analysis, we focused on the relationship between the thermal contrasts in TP-TIO region and the SASM circulation in summer because the meridional thermal contrast is the most obvious and the atmospheric baroclinicity is the greatest.

The outgoing longwave radiation (OLR; period: 1979–2019; resolution: 2.5° × 2.5°) data were obtained from NOAA (the National Oceanic and Atmospheric Administration) (Liebmann and Smith, 1996), and the precipitation data from NOAA's CMAP (Climate Prediction Center Merged Analysis of Precipitation; period: 1979–2019; resolution: 2.5° × 2.5°) (You et al., 2015). The surface air temperature was obtained from NASA's GISS (Goddard Institute for Space Studies) data set (period: 1979–2019; resolution: 2° × 2° (Hansen et al., 2010)) and ERA5 (period: 1979–2019; resolution: 1° × 1°) data.

2.2 Methods

1) Indirect method

The AHS and AMS are the atmospheric diabatic heating, of which the AMS represents the precipitation condensation heating. The AHS is also referred to as the "apparent" heat source, resulting from resolved motion heating, so we can think of it as the sum of surface sensible heating, condensation heating, and radiative heating. Direct and indirect methods can both be used to obtain the AHS and AMS (Luo and Xu, 2019), wherein the indirect method is also called the "residual diagnosis method." The present study used the indirect method (Yanai et al., 1992) to obtain the vertical structure of the AHS and AMS with reanalysis data. We use Q_1 and Q_2 to represent the AHS and AMS, respectively. $< Q_1 >$ and $< Q_2 >$ are defined by Eqs. (1) and (2), which is the sum of the time tendency term, the advection variation term, and the vertical variation term. According to Eqs. (1) and (2), we can calculate the Q_1 and Q_2 at each layer, also known as the heating rate (units: K/day):

$$< Q_1 > = \frac{c_p}{g}\int_{P_T}^{p_s}\left[\left(\frac{p}{p_0}\right)^k\left(\frac{\partial\overline{\theta}}{\partial t}+\vec{V}\cdot\nabla\overline{\theta}+\overline{\omega}\frac{\partial\overline{\theta}}{\partial p}\right)\right]\mathrm{d}p, \tag{1}$$

$$< Q_2 > = -L\frac{c_p}{g}\int_{P_T}^{p_s}\left[\left(\frac{\partial\overline{q}}{\partial t}+\vec{V}\cdot\nabla\overline{\theta}+\overline{\omega}\frac{\partial\overline{q}}{\partial p}\right)\right]\mathrm{d}p. \tag{2}$$

In the above equations, $< > = \frac{1}{g}\int_{P_T}^{p_s}()\mathrm{d}p$,; the overbars represent regional average values; θ and q are potential temperature (unit: K) and specific humidity (units: g/kg), respectively; $\vec{V}$ and ω are horizontal wind speed (units: m/s) and vertical velocity (units: Pa/s); p_s and p_T are surface and top-of-the-atmosphere pressure, respectively; C_D = 0.004 is the specific heat of dry air at constant pressure; g = 9.8 m/s^2 and k = 0.286; $L = 2.5 \times 10^6$ J/kg is the condensation heating coefficient; and ∇ is the horizontal gradient operator.

For convenience, we use Q_1 represent $< Q_1 >$ and Q_2 to represent $< Q_2 >$ hereafter. When Q_1 is greater (less) than zero, it indicates that the atmosphere has a net heat gain (loss). Generally, a positive value of Q_1 is called a heat source and a negative value a heat sink. When Q_2 is greater (less) than zero, it means there is a net mositure loss (gain). If the spatial distributions of Q_1 and Q_2 are consistent and both positive, this indicates that the AHS is mainly dominated by precipitation latent heating.

2) Thermal contrast indexes

The present study obtained the monthly mean Q_1 and Q_2 during 1979–2019 with ERA5 data. Few studies have used the AHS to represent land–sea heating contrast. The standardized values of the meridional thermal contrast, based on the integral of Q_1 on the whole layer, is defined as QI (Eq. (3)). It represents the difference of the whole atmospheric column heating between the TP (75°E–103°E,

28°N–38°N; altitude⩾3000 m) and TIO (60°E–100°E, 15°S–5°N). Besides, QI_{up} (Eq. (4)), TI_{up} (Eq. (5)) and TI_{s} (Eq. (6)) were also defined, to depict the meridional thermal contrast:

$$QI = (Q_{1TP} - Q_{1TIO})_{1000-100\ \mathrm{hPa}}, \tag{3}$$

$$QI_{\mathrm{up}} = (Q_{1TP} - Q_{1TIO})_{400-200\ \mathrm{hPa}}, \tag{4}$$

$$TI_{\mathrm{up}} = (T_{TP} - T_{TIO})_{400-200\ \mathrm{hPa}}, \tag{5}$$

$$TI_s = (T_{TP} - T_{TIO})_{2\ \mathrm{m}}. \tag{6}$$

Temperature is a comprehensive manifestation of thermal conditions. Using the AHS to describe the land–sea thermal contrast can better reflect the evolution of thermal conditions. Zhang et al. (2017) defined the meridional land–sea thermal difference by using the AHS, which can be used to investigate the onset of the SASM. QI, QI_{up}, TI_{up} and TI_{s} are all land–sea thermal contrasts, but they have different emphases on describing the thermal differences.

3) Atmospheric baroclinic component

The atmospheric kinetic energy of the vertical mean flow (u_{m}, v_{m}) and the shear flow (u_{s}, v_{s}) can be referred to as the barotropic and baroclinic component, respectively (Eqs. (7) and (8)). The present study used the vertical shear flow to define the atmospheric baroclinicity. K_s (Eq. (9)) is the result of the vertical integration of baroclinicity, which can be divided into zonal shear energy (K_{su}) and meridional shear energy (K_{sv})(Xu and Chan, 2002) :

$$u = u_{\mathrm{m}} + u_{\mathrm{s}}v = v_{\mathrm{m}} + v_{\mathrm{s}}, \tag{7}$$

where

$$(\ )_m = \frac{1}{p_0 - p_t}\int_{p_t}^{p_0} \mathrm{d}p, \tag{8}$$

$$K_s^2 = \frac{1}{2g}\int_{p_t}^{p_s} (u_s^2 + v_s^2)\mathrm{d}p. \tag{9}$$

p_s and p_{T} are surface and top-of-the-atmosphere pressure, respectively. The monsoon is significantly affected by the land–sea thermal difference. The prevailing wind direction in the monsoon region not only has a seasonal reversal, but also has a significant change in wind direction in the vertical direction. Based on this basic understanding, defining the K_s to measure the strength of baroclinic atmospheric motion can reveal some basic properties of the monsoon (Guan, 2000).The larger (smaller) the value of K_s, the stronger (weaker) the intensity of the SASM.

4) South Asian monsoon index

According to the definition in a previous study (Xu and Chan, 2002), the total shear energy of K_s over the SAM region can be defined as the Monsoon Index (*MI*) (Eq. (10)), which is the standardized value. The correlation of the summer *MI* with WYI (Webster and Yang, 1992) reaches 0.95, in which WYI is defined by the zonal wind difference between 850 and 200 hPa over the region (0°–20°N, 40°–110°E). The larger (smaller) the value of , the stronger (weaker) the intensity of the SAM:

$$MI = \int_A K_s \mathrm{d}A. \tag{10}$$

5) Statistical methods

Correlation analysis, synthetic analysis, linear regression analysis, and the *t*-test were used as statistical methods in this research. For further details regarding these methods, please refer to Huang and Li (2015).

3 Thermal contrast between the TP and TIO region

3.1 Q_1 and K_s

The seasonal conversion of the AHS in the Asian monsoon area is obvious, and the intensity of the summer AHS is the strongest, resulting from the precipitation condensing heat. The strongest values ($Q_1 \geqslant 300$ W/m^2) are located over the Bay of Bengal (BOB) and the southern TP, and the second strongest ($Q_1 \geqslant 150$ W/m^2) over the central and eastern TP, the TIO, the Indochina Peninsula, the west and north of the Indian Peninsula, and the eastern and southern Yungui Plateau (Fig. 2). In summer, the TP AHS reaches its strongest at the same latitude, and the TIO is the weakest, so the thermal contrast is the greatest between the TP and TIO (Fig. 3). The horizontal distribution (not shown) of the AMS in the TP–TIO region is basically consistent with the distribution of the AHS in summer, which indicates that the heating in the TP–TIO is mainly dominated by condensation latent heat.

Due to the seasonal reversal of the prevailing wind direction and the change of upper winds, the atmospheric baroclinicity in the monsoon region is strong, especially in summer and winter. The strong baroclinic zone ($K_{\mathrm{s}} \geqslant$ 60 m/s) in spring, autumn and winter is located near 25°N, which splits into the westerly zone and the SAM zone in summer. The K_{s} in the SAM is the strongest, with the strongest center (near the Somalia jet) reaching 100 m/s (Fig. 2). The strong westerly baroclinic zone at mid-latitude exists throughout the year, and reaches the weakest in summer (Fig. 2), which is related to the jet and the baroclinic front in the upper troposphere (Guan, 2000). However, the kinetic energy of baroclinic movement in the Asian-Australian monsoon region is stronger, and reaches the strongest in summer (Fig. 2). There are opposite zonal

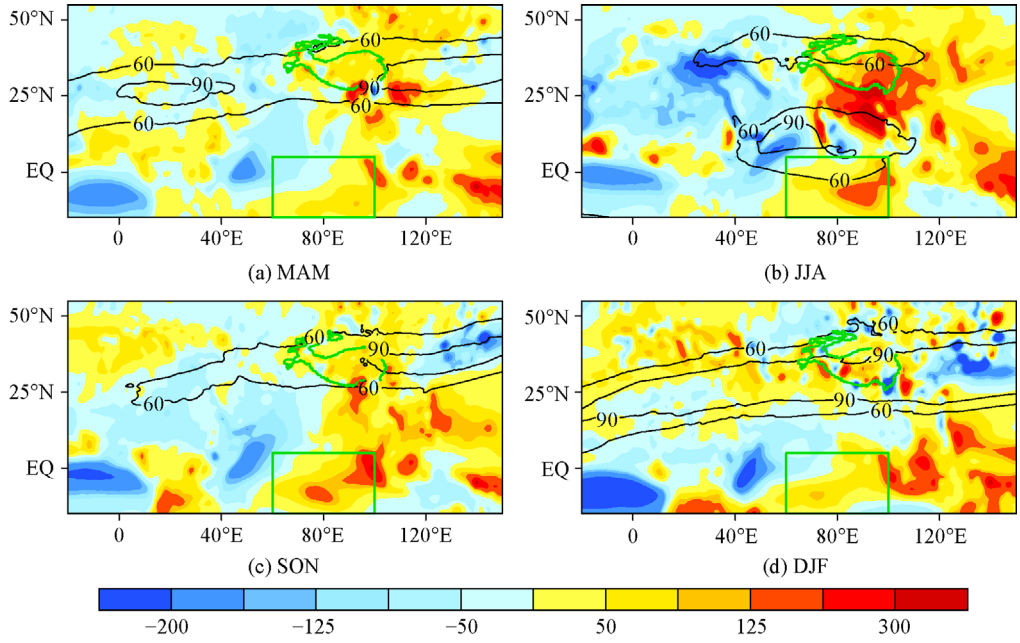

Fig. 2 Seasonal variations of the zonal anomaly of $Q1$ (shaded; units: W/m^2) and $K_s \geqslant 60$ m/s (black curve). MAM (March–April–May), JJA (June–July–August), SON (September–October–November) and DJF (December–January–February) represent spring, summer, autumn and winter, respectively. The Tibetan Plateau ($\geqslant$3000 m) is outlined in green; the tropical Indian Ocean is indicated by the green box.

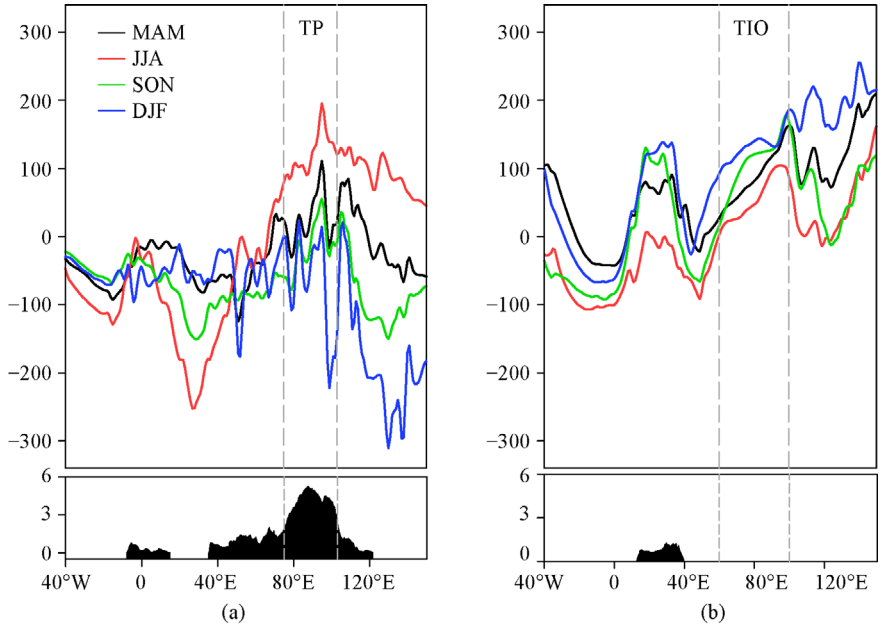

Fig. 3 Zonal mean of (a) $Q1$ and (b) $Q2$ (units: W/m^2). The Tibetan Plateau (TP$\geqslant$3000 m) is located at 28°N–38°N; the tropical Indian Ocean (TIO) is located at 15S°–5°N; MAM (March–April–May), JJA (June–July–August), SON September–October–November) and DJF (December–January–February) represent spring, summer, autumn and winter, respectively; and altitude is shaded black (unit: km).

wind components in the upper and lower troposphere in SASM region, at the same time the zonal baroclinic movement is dominant, so the baroclinicity is the strongest ($K_s \geqslant 90$ m/s) in summer. The TP and TIO are respectively located in the north and the south of the strong monsoon baroclinic zone in the meridional direction. The range of atmosphere baroclinicity in Asia can represent the monsoon range (Guan et al., 1997), so the SAM index,

MI, was constructed in the present study based on the atmosphere baroclinicity.

3.2 Summer vertical profiles of Q_1 and Q_2

To identify the main factor contributing to the atmospheric heating, we analyzed the vertical structure of Q_1 and Q_2. In Fig. 4(a), Q_1 is greater than 0, indicating that the TP and TIO are both a heat source in summer. The TIO Q_1 increases significantly with height, with the height of maximum heating at 400 hPa (1.5 K/d), while the TP Q_1 is greater (about 3 K/d) below 300 hPa, which is the same as the result from observation (Yanai et al., 1992) and reanalysis (Yanai and Tomita,1998) data. The vertical transportation plays a leading role for the Q_1 and Q_2 above 900 hPa, which are both greater than 0. The heights of maximum heating between Q_1 and Q_2 are inconsistent, indicating that Q_1 is mainly convection condensation heating (Yanai and Tomita, 1998). Due to the evaporation and horizontal advection in the low-level troposphere, the TIO becomes a moisture source below 900 hPa. In summer, there is a large heating center at 10°N–30°N (Fig. 5(a)), which corresponds to the warm center over the southern TP (Fig. 5(d)). The horizontal advection in the upper troposphere changes little in the meridional direction (Li and Yanai, 1996) and zonal direction (Duan and Wu, 2005), and Figs. 5(a) and 5(c) also show the main contribution of Q_1 comes from precipitation condensation heating in the monsoon region.

The heat source center of the BOB corresponds to the strong convection activity center (OLR$\leqslant$200 W/m^2), while the strong heat source center of the TP corresponds to the sub-strong convection activity center (OLR$\leqslant$ 210 W/m^2) (Figs. 2(b) and 6). Figure 5 shows that there are two heating centers in summer in the upper troposphere, which are located on the SAM region and the TP, respectively.

The summer spatial distribution of Q_1 at 400–200 hPa is the same as the integral of the whole layer (Fig. 2(b)). According to the above analysis, the summer Q_1 in the TP–TIO region is dominated by deep convection heating, with the strongest intensity in the upper troposphere.

The east and west sides of 65°E are abnormal heat sources and cold sources, respectively (Fig. 2(b)), which correspond to strong convection heating and radiative cooling. Atlantic-Africa-Eurasia-Pacific region (AAEP) in summer is the quadruple heating pattern. A strong LO (longwave radiative cooling) lobe is located over eastern North Atlantic. A SE (diffusive sensible heating) lobe occupies the vast western and central AAEP area. A very intense CO (deep convective heating) lobe is found over the East Asian monsoon (Wu and Liu, 2003). Figure 2(b) shows the SE and CO of the AAEP. Because the atmospheric net radiative cooling in the Mediterranean and the Arabian Sea is stronger than the sum of sensible heating and latent heating, these two places are powerful air-cooling sources (Fig. 2(b)). The sensible heating on the surface of northern Africa plays a leading role, while the latent heating of condensation and the net radiative cooling of the atmosphere are very small, so it is a weak heat source (Wu and Liu, 2003). Since the Asian monsoon region is heated by strong convection heating, the zonal abnormal

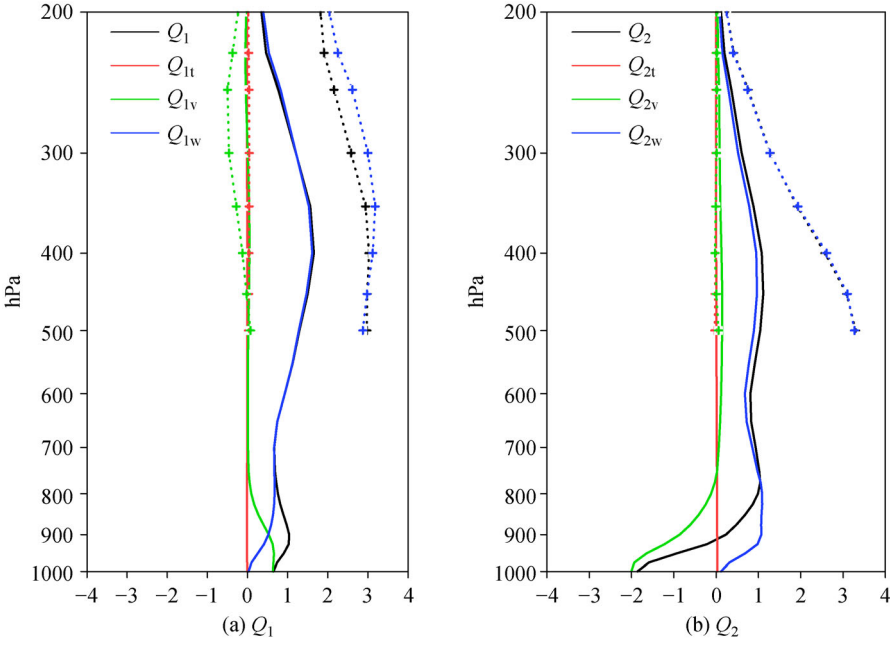

Fig. 4 Vertical profiles of summer Q_1 and Q_2 at 90°E. The Tibetan Plateau is represented by the dotted curve at 28°N–38°N, and the TIO by the solid curve at 15°S–5°N; Q_{1_t}, Q_{1_v} and Q_{1_w} represent the time tendency, horizontal advection and vertical advection, respectively, and likewise for Q_2.

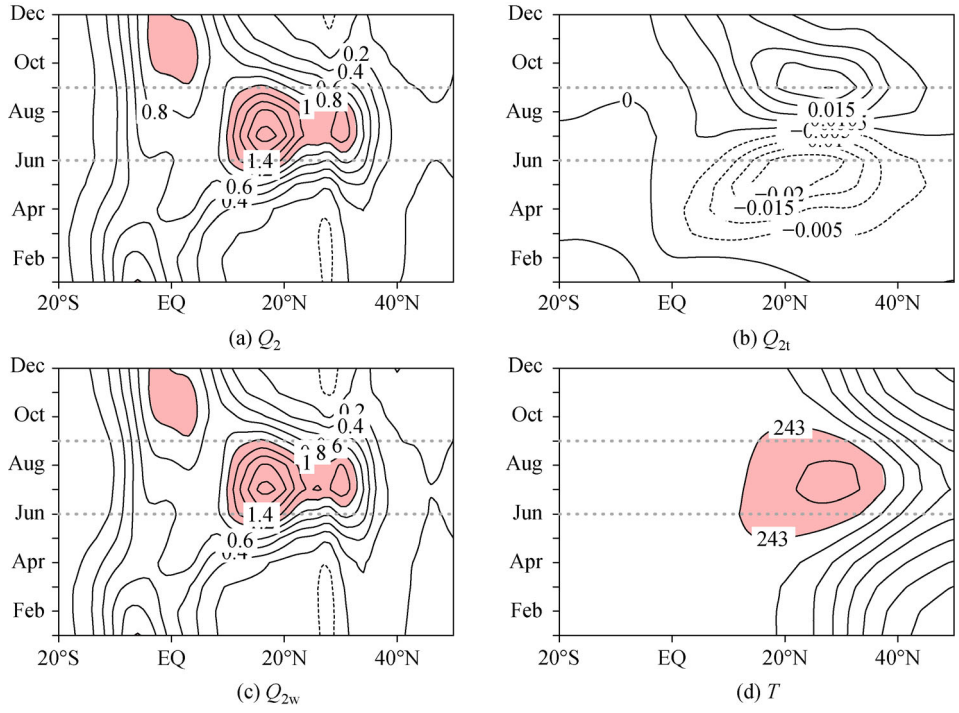

Fig. 5 The 400–200-hPa time–meridional variations of (a) Q_2, (b) Q_{2t}, (c) Q_{2w} and (d) temperature at 70°E–100°E(Q_{2t}, and Q_{2w} represent the time tendency and vertical advection, respectively).

value of the heat source shows that most of the central and western parts of the AAEP are abnormal cold sources (Fig. 2(b)).

Based on T–Q_Z theory (Wu et al., 2016) and thermal wind theory (Holton and Hakim, 2004; Dai et al., 2013), the north (south) wind shear is formed above the heating (cooling) zone and the warm (cold) center is located on the west side of the heating (cooling) zone, which results in the strong warm center and SAH (geopotential ⩾ 12500 gpm) (Wei, 2015) in the upper troposphere (Fig. 6). The Q_1 in the TP–TIO area is dominated by deep convection heating, and the warm center is located on the west side of the monsoon heating zone. The location of the warm center

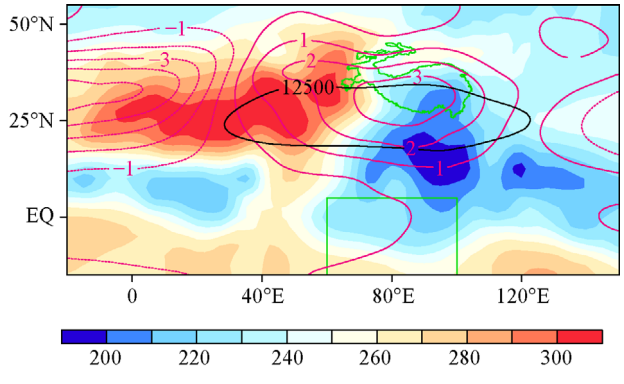

Fig. 6 Zonal temperature anomaly at 400–200 hPa (red curve, unit: K), 200-hPa geopotential ⩾ 12500 gpm (black curve), and outgoing longwave radiation (shaded; units: W/m^2) in summer. The Tibetan Plateau (⩾ 3000 m) is outlined in green; the tropical Indian Ocean is indicated by the green box.

($T \geqslant 1$ K) is between the TP and TIO, which coincides with the location of the SAH. The SAH is a large anticyclonic circulation system in the upper troposphere and lower stratosphere in the Asian monsoon region in the northern hemisphere in summer. The interaction between the SAH in summer and other systems, especially the interaction with the SASM, East Asian summer monsoon and precipitation, has an important impact on the evolution of atmospheric circulation throughout the northern hemisphere and the Asian monsoon region. The abnormal heating in the Asian monsoon region will cause abnormal intensity or position of the SAH. It is also found that the southern boundary of the SAH is near 18°N, the northern boundary is in the middle of the TP, and the eastern ridge point is near Taiwan Island (Fig. 6).

3.3 Seasonal variations of the thermal contrast indexes and monsoon index

The seasonal changes of the AHS over the TP and TIO are opposite, wherein in the summer the TP is the strongest and the TIO is the weakest, so the thermal contrast is the most obvious (Fig. 7).

The seasonal variations of QI, QI_{up}, TI_{up} and MI are basically the same, and QI and MI increase significantly in June, with the greatest increase in summer and the largest in July. The curve of QI is the same as that of QI_{up}, which further proves that the TP–TIO region is mainly dominated by deep convection heating in the upper troposphere. The QI changes from negative to positive in March–April, while the conversion of TI_{up} and MI lags by one and two

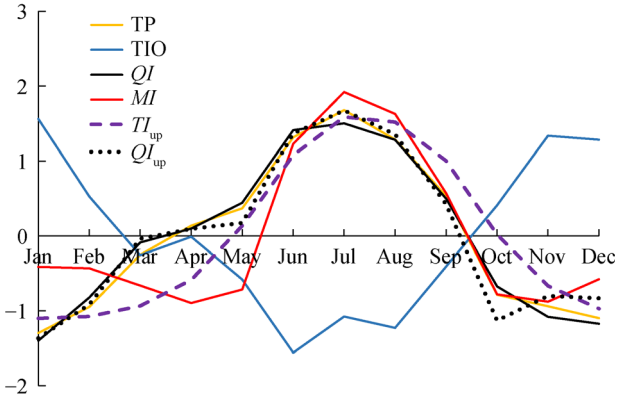

Fig. 7 Seasonal variations of QI (solid black line), QI_{up} (black dotted line), TI_{up} (purple line) and MI (red line) (see subsection 2.2 (2) in the main text for definitions of these indexes). The Q_1 in the TP and TIO is denoted in orange and blue, respectively, and all data have been detrended and standardized.

months, respectively, and the three indexes all change from positive to negative in September–October. Since the thermal contrast in summer is the most obvious in the TP–TIO region, the present study focuses on the relationship between the meridional thermal contrast in summer and the SAM circulation. In addition, the value of MI in summer is significantly larger than that in winter, so the intensity of the SAH is much stronger than that of the winter monsoon. The impact of the meridional gradient of the TP–TIO heat source on the development and evolution of the SASM in the transition seasons needs further study in the future.

Based on the above analysis, it can be seen that the TP and TIO regions are both heat sources in summer, and mainly deep convection heating, which reaches its strongest level in the upper troposphere. The seasonal changes of Q_1 in the two regions are reversed, with the strongest in the TP and the weakest in the TIO in summer, so the thermal contrast is the strongest. The TP (TIO) heat source locates in the north (south) of the strong baroclinic zone, the SAH and the warm center in the upper troposphere. The strong TP–TIO heat source can strengthen the SAH and the upper-tropospheric warm center. The seasonal variations of QI are the same as those of MI, indicating that the strong intensity of the meridional thermal contrast in summer corresponds to the strong SASM.

4 Variations of the SASM and the meridional thermal contrast anomaly

4.1 Evolutionary characteristics of the SASM

Precipitation increases significantly in the BOB in early May, indicating the onset of the SASM (Wu et al., 2012). At the same time, the south-western airflow in Somalia near 45°N is established in the lower atmosphere, which is affected by the Coriolis force to turn into a westerly wind near the Arabian Sea. In June, westerly winds increase rapidly, reaching their maximum in July, and then gradually weaken in September. The atmospheric baroclinicity (K_s) and precipitation in the SAM area also have similar evolutionary processes, but are affected by the distribution of the land and sea; the intensity and extent of precipitation on the west side of the Indian Peninsula and Indochina Peninsula are greater than those on the east side (Fig. 8). After monsoon onset, the low upper troposphere of the SAM area is the westerly jet (the strongest center is at 62°E) and the upper is easterly winds (the strongest center is at 95°E), while the atmospheric baroclinicity reaches its strongest in the SAM area. The precipitation over the BOB is the greatest in the SAM.

From the seasonal–zonal profiles (Fig. 9), it can see that the Q_1 and precipitation reach their maximums in summer, with larger values on the west side of the Indian Peninsula (80°E) and the Indochina Peninsula (100°E), resulting from the land–sea distribution. Next, we analyzed the temperature and the baroclinicity in the TP–TIO area when the summer meridional thermal contrast is abnormal.

4.2 Selection of abnormal thermal contrast years

The QI, QI_{up}, MI and TI_{up} all have interdecadal increasing trends, so all data were detrended and standardized (Fig. 10). The years of abnormal QI do not possess one-to-one correspondence with those of abnormal TI_{up}, QI_{up} and MI. The correlation coefficients between QI and TI_{up}/QI_{up}/MI are 0.337, 0.634 and 0.407, respectively, the correlation coefficients between MI and TI_{up}/QI_{up} are 0.736, and 0.501, respectively (all correlation coefficients pass the 95% significance test). However, the correlation coefficients between TI_{up}, and QI_{up}, QI and TI_s is 0.204 and 0.101, respectively (the value does not pass the 95% significance test). The correlation analysis demonstrates that the relationship between QI and TI_{up} is closer, and the intensity of SASM (MI) has a strong relationship with the temperature gradient between the TP and TIO in the upper troposphere. Considering that the land–sea thermal contrast in the TP–TIO area is also affected by the sensible heating near the ground, we defined the summer QI being greater than (less than) one standard deviation as years when the meridional thermal contrast is abnormally strong (weak). Accordingly, the strong years ($QI \geqslant 1$) are 1980, 1985, 1990, 1991, 2011, 2012 and 2018; and the weak years ($QI < 1$) are 1979, 1989, 1995, 1996 and 2002 (Fig. 10).

4.3 Temperature anomalies in the upper troposphere

The distribution of temperature in the upper troposphere is opposite when the thermal contrast between the TP and TIO is abnormal (Fig. 11). The boundary between the

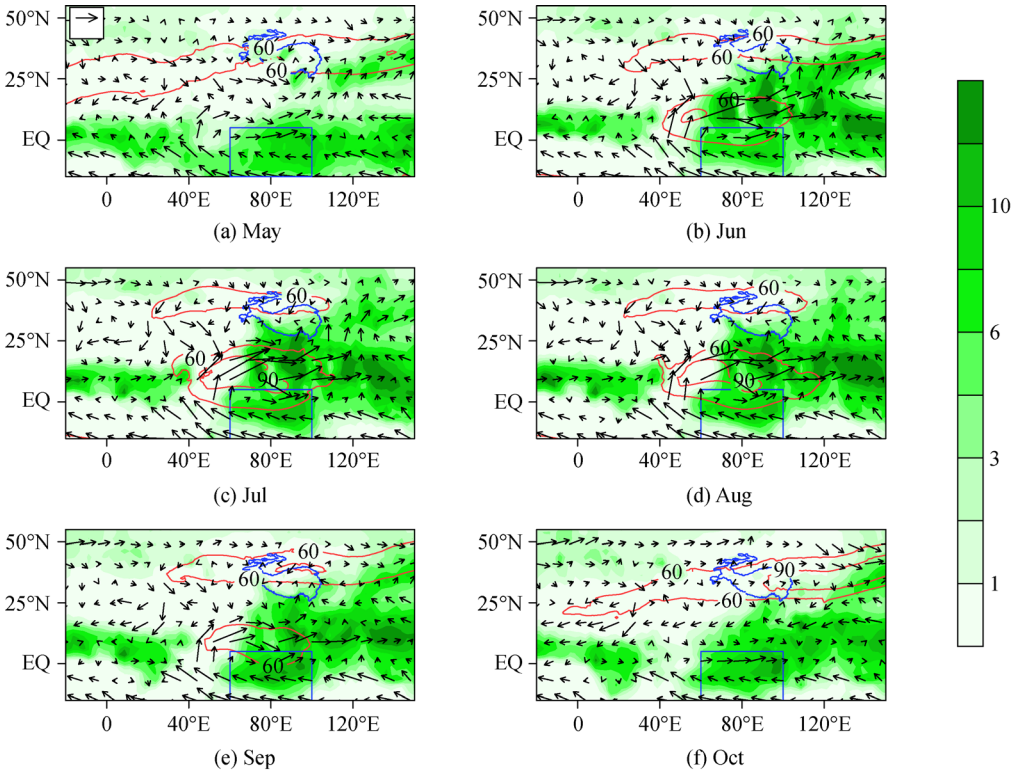

Fig. 8 Evaluation of the SASM, in which (a–f) represent May–October, respectively, with precipitation shaded (units: mm/day). The wind vectors are at 850 hPa (units: m/s); the $K_s \geqslant 60$ m/s is outlined in red; the Tibetan Plateau is outlined in blue (altitude $\geqslant 3000$ m); and the tropical Indian Ocean is denoted by the blue box.

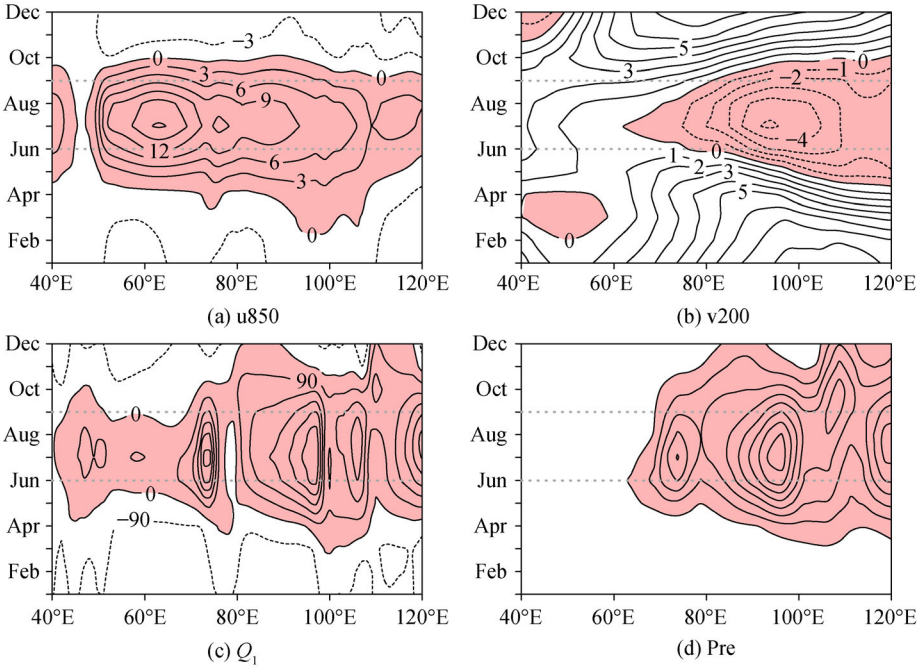

Fig. 9 Seasonal–zonal profiles at 15°N of (a) zonal wind at 850 hPa, (b) meridional wind at 200 hPa, (c) Q_1, and (d) precipitation. Shading in (a, c) represents values $\geqslant 0$; in (b) it represents $v \leqslant 0$; and in (d) Pre $\geqslant 0$.

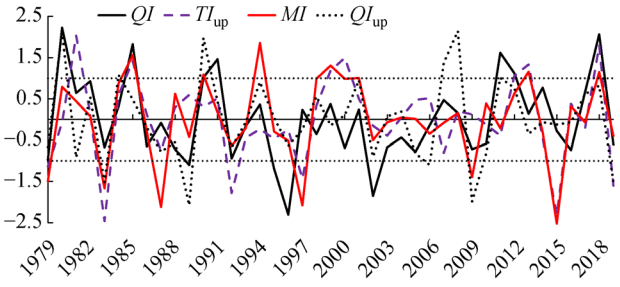

Fig. 10 Temporal variations of the summer QI, TI_{up}, QI_{up} and MI (see section 2.2. (2) for definitions of these indexes; all data have been detrended and standardized).

abnormal cold and warm regions is near 18°N, which is south of the SAH and north of the strong baroclinic zone. When the QI is abnormally high (low), Eurasia and northern Africa are warmer (colder), and the TIO colder (warmer), resulting in the meridional temperature gradient being significantly larger (smaller) (Fig. 12). The thermal wind relationship reveals that the zonal (meridional) wind shear is determined by the meridional temperature gradient. According to thermal wind theory, easterly (westerly) winds occur when the north is warm (cold) and the south is cold (warm). Hence, it can be speculated that the intensity of the anticyclonic circulation of the SAH would be strengthened (weakened) by the abnormally high (low) thermal contrast between the TP and TIO. In addition, it was also found that, when QI is high, the range of $K_s \geqslant 60$ m/s extends to the south of the South China Sea, and $K_s \geqslant 90$ m/s extends from the Arabian Sea to the southern part of the BOB. This indicates that the baroclinicity is enhanced in the SAM. When QI is low, the range of the strong baroclinic area is smaller.

4.4 Summer atmospheric baroclinic anomalies in the TP–TIO region

There are abnormal heat sources over the land and abnormal cold sources over the sea when QI is

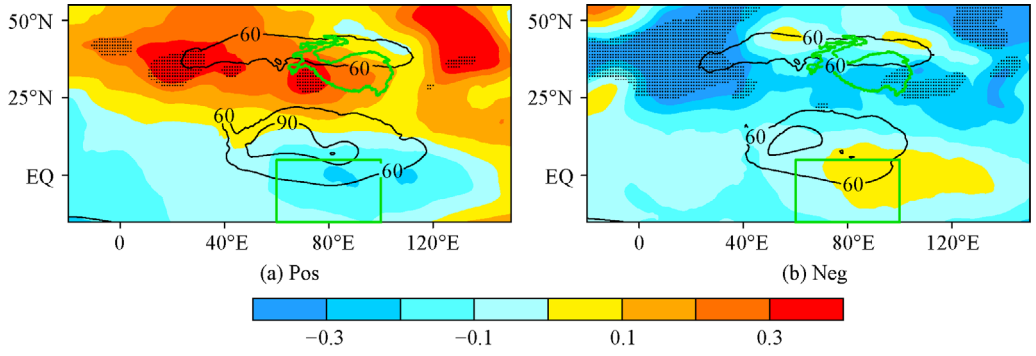

Fig. 11 Anomalous temperature at 400–200 hPa (shaded; unit: K; dotted areas pass the 90% significance test) and K_s ($\geqslant$60 m/s). Pos represents $QI \geqslant 1$; Neg represents $QI < 1$. The Tibetan Plateau ($\geqslant$3000 m) is outlined in green; the tropical Indian Ocean is denoted by the green box.

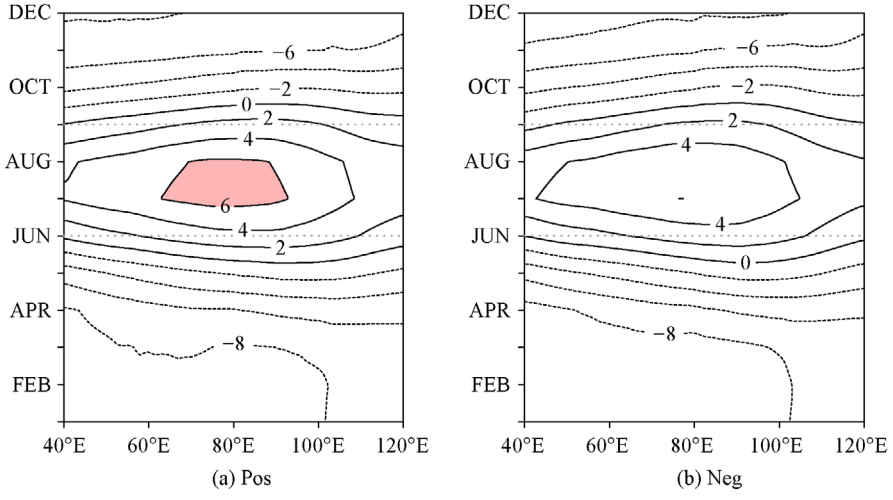

Fig. 12 Seasonal profiles of the difference in anomalous temperature at 400–200 hPa between 30°N and 5°N. Pos represents $QI \geqslant 1$; Neg represents $QI < 1$; shaded area represents temperature $\geqslant$ 6 K.

anomalously high. The atmospheric baroclinicity in the SAM area is enhanced, the strong center is located at 600 hPa, and the strong heat source and cold source centers are both located at 450 hPa. When *QI* is anormaly low, the distribution is almost the reverse (Fig. 13). However, in other seasons the meridional thermal contrasts in the TP-TIO region and the atmospheric baroclinicity of the SAM region have no obvious reverse characteristics. The *u*-component of the K_s in the SAM area is about three times larger than the *v*-component, so the increase in K_s is mainly due to the increase in the *u*-component (Table 1).

In the years of anomalously high *QI*, the meridional thermal contrast between the TP and the TIO strengthens in summer and the meridional temperature gradient increases in the upper troposphere. Eurasia is warmer and the TIO is colder. There is an anomalous warm center over the west of the TP. At the same time, tropospheric baroclinicity is enhanced, contributed mainly by the increase in the *u*-component. In the years of anomalously low *QI*, the situation is basically the opposite.

5 Relationship between the TP–TIO thermal contrast and the SASM in summer

5.1 Correlation between thermal contrast indexes and *MI*

Monthly data were used in this part of the study to perform correlation analyses. *QI* and *MI* have the strongest positive contemporaneous correlation (correlation coefficient of 0.729; Table 2), which means that the strong thermal contrasts between the TP and TIO is linked with a strong SASM. The correlation between *QI* and TI_{up} is one month ahead, with a correlation coefficient of 0.841. This one-month-lead correlation coefficient between *QI* and TI_{up} is the largest (0.841).

5.2 Relationship between the TP–TIO thermal contrast and the TI_{up}, *MI* and K_s in summer

The TI_{up} regression coefficients are significantly positive in the upper troposphere over the Mediterranean, Iranian

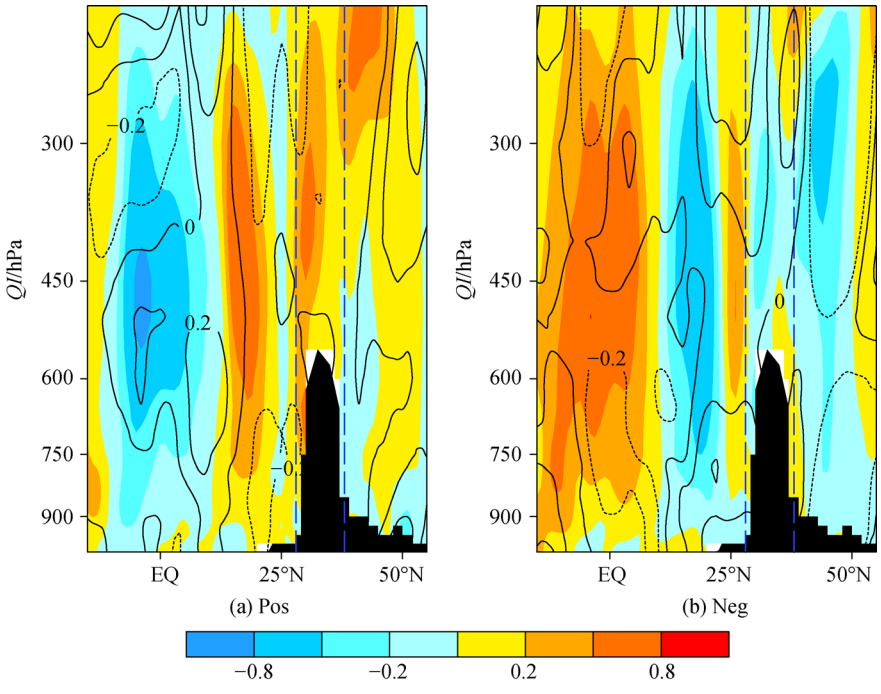

Fig. 13 Vertical–meridional profiles of the anomalous Q_1 (shaded) and K_s (curve) in summer. The mean is at 80°E–96°E; Pos represents $QI \geqslant 1$; Neg represents $QI < 1$; and black shading and blue dotted line represent the topography and TP respectively).

Table 1 The anomalies of K_{su} and K_{sv} in summer. Pos represents $QI \geqslant 1$; Neg represents $QI < 1$; Nor represents the normal.

	K_{su}			K_{sv}		
	Nor	Pos	Neg	Nor	Pos	Neg
Jun	66.40	70.53	66.40	19.98	21.23	19.15
Jul	80.10	80.84	80.10	22.19	22.37	21.17
Aug	74.74	78.00	74.74	19.98	21.11	19.44
mean	73.75	76.45	73.75	20.71	21.57	19.92

Table 2 Correlation coefficients between the thermal contrast index and *MI*

	QI			
	+ 3	+ 2	+ 1	0
MI	0.158	0.412	0.642	0.729
TI_{up}	0.327	0.659	0.841	0.796

Notes: all data were detrended and standardized; + 3, + 2 and + 1 represent leads of 3 months, 2 months and 1 month of *QI*, respectively; and 0 represents simultaneous correlation analysis.

Plateau and western TP (Fig. 14(a)), while the T_{2m} regression coefficients are significantly negative over the BOB, central and southern South China Sea, Arabian Sea, and northern part of the Indian Peninsula (Figs. 14(c) and 14(d)). These results indicate that the greater the value of *QI*, the warmer the upper troposphere over the Iranian Plateau and surrounding areas, and the colder it is at the surface of the BOB, central and southern South China Sea, Arabian Sea, and northern part of the Indian Peninsula. The K_s regression coefficients are significantly positive (Fig. 14(b)), implying that the meridional thermal contrast has a significant positive contribution to baroclinicity in the SAM area. However, in other seasons the relationship between the TP–TIO thermal contrast and the TI_{up}, *MI* and K_s have no significance characteristics.

The above analysis shows that the responses of lower and upper temperature in the Asian monsoon region to meridional thermal contrast are different. Because the atmospheric heating in the TP–TIO area is dominated by deep convection heating, the meridional anomaly of the heat source should first affect the temperature in the upper troposphere. Consequently, the abnormal thermal contrast (that is, anomalous *QI*) leads to an abnormal meridional temperature gradient in the upper troposphere, which can affect the atmospheric baroclinicity and monsoon circulation anormaly. Ultimately, the anomalous monsoon precipitation might result in abnormal temperatures at the surface.

5.3 Years of anomalous monsoon circulation

The westward airflow over the east coast of Africa in the lower troposphere increases over the Arabian Sea, Indian Peninsula, and BOB, which converges with the anomalous anticyclone of the North-west Pacific in the Indochina Peninsula during the abnormally high *QI*. In the upper troposphere, the northerly winds increase, the monsoon region is dominated by easterly winds, and there are abnormal northerly winds in the large heat source area of the eastern TP (Figs. 15 and 16). Analyzing the profiles of *u*–*w* wind, it can be seen that the Walker circulation strengthens in the equatorial Indian Ocean (Fig. 17). In the years of anomalously low *QI*, the circulation is almost the opposite. However, there are no obvious abnormal southerly winds at 200 hPa over the east of the TP (Fig. 16(b2)), which is related to the abnormal meridional distribution of the heat sources over the TP (Fig. 13(b)). When the *QI* is abnormally low, the abnormal cold source at the middle-upper troposphere in the middle-eastern of the TP is weak, so the anomalous southerly wind over the cold source is weaker.

5.4 Difference in anomalous precipitation

In years of anomalous *QI*, the distribution of abnormal precipitation is significant. The enhanced monsoon circulation results in increased monsoon precipitation when *QI* is abnormally high. The difference in precipitation in the Asian monsoon region between positive and

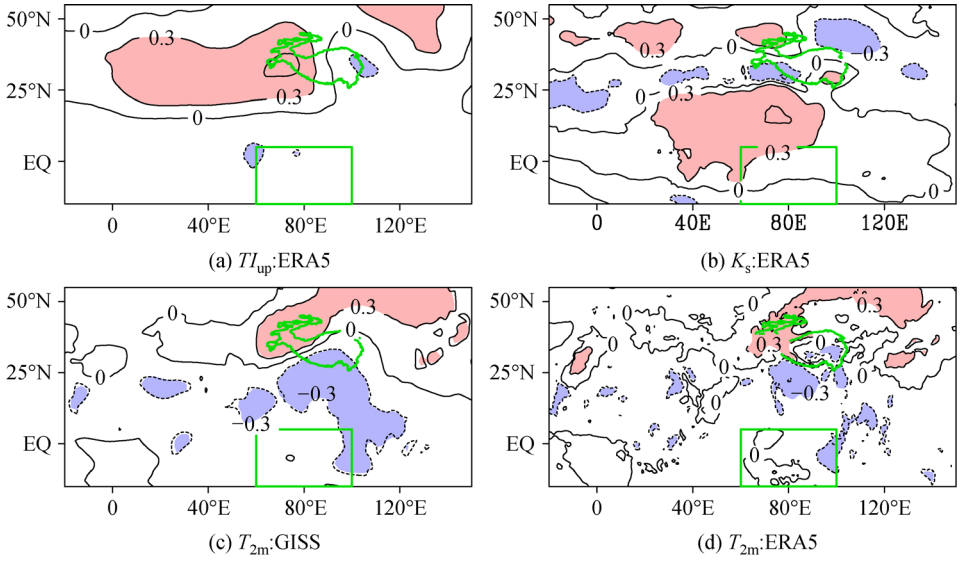

Fig. 14 Regression of TI_{up}, K_s and T_{2m} on *QI* in summer. Shaded areas pass the 95% significance test; the Tibetan Plateau (⩾3000 m) is outlined in green; and the tropical Indian Ocean is denoted by the green box.

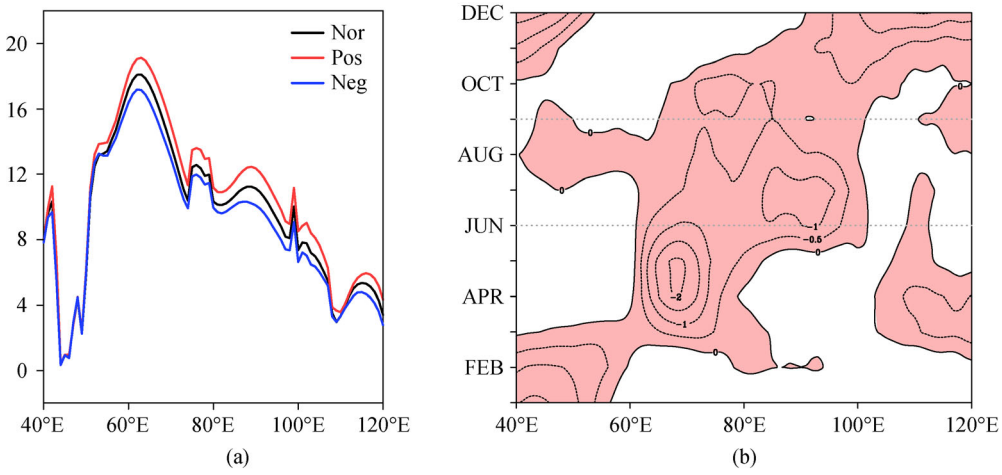

Fig. 15 The 850-hPa *u*-component (a) and 200-hPa *v*-component in summer at 15°N (b). Pos represents $QI \geqslant 1$; Neg represents $QI < 1$; Nor represents the norm; and shading indicates $v \leqslant 0$.

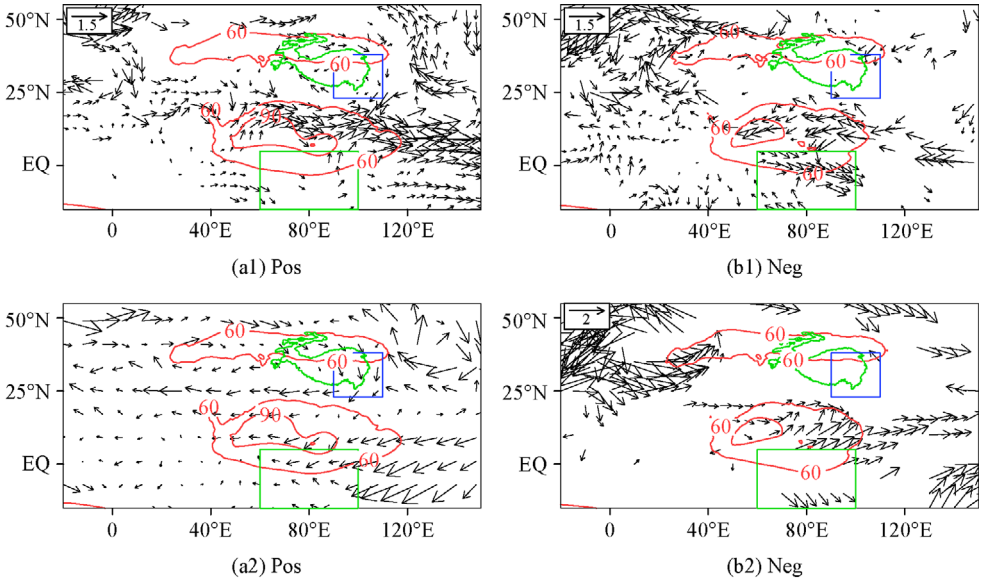

Fig. 16 Abnormal winds at 850 hPa (a1, b1), 200 hPa in summer (a2, b2) and the K_s (red curve). Pos represents $QI \geqslant 1$; Neg represents $QI < 1$; wind vectors pass the 95% significance test; the Tibetan Plateau (≥3000 m) is outlined in green; the tropical Indian Ocean is denoted by the green box; and blue box represent 90°E–110°E, 23°N–38°N.

negative *QI* shows that the BOB, Indochina Peninsula, the north of Indian Peninsula, Philippines and the north-western Pacific have more precipitation, while the precipitation over the central and eastern TIO and the eastern China are relatively weaker. The major mode of the composite of precipitation anomaly consists of a bimodal meridional structure between the SASM region and the TIO region, and a bimodal structure between the SASM region and the north-western Pacific (Fig. 18). The distribution of abnormal precipitation is almost consistent with the previous study (Goswami et al., 1999). We also found that when the *QI* index is too large, the area and intensity of SAH increased significantly (Fig. 18), but the center position does not change much.

Correlation analysis shows that the thermal contrast between the TP and TIO has a significant positive correlation with *MI*. When *QI* is abnormally high, the upper troposphere over Eurasia is warmer and the TIO is colder, and a warm center locates over the west side of the TP. Due to the upper temperature in summer being mainly affected by diabatic heating, the meridional temperature gradient also increases. The increased thermal meridional gradient leads to enhanced atmospheric baroclinicity. Hence, the low-level abnormal westerly airflow and the upper-level abnormal easterly airflow strengthen the intensity of the Walker circulation, resulting in much more precipitation over the SASM region. This strengthened surface precipitation leads to a decrease in the 2-m

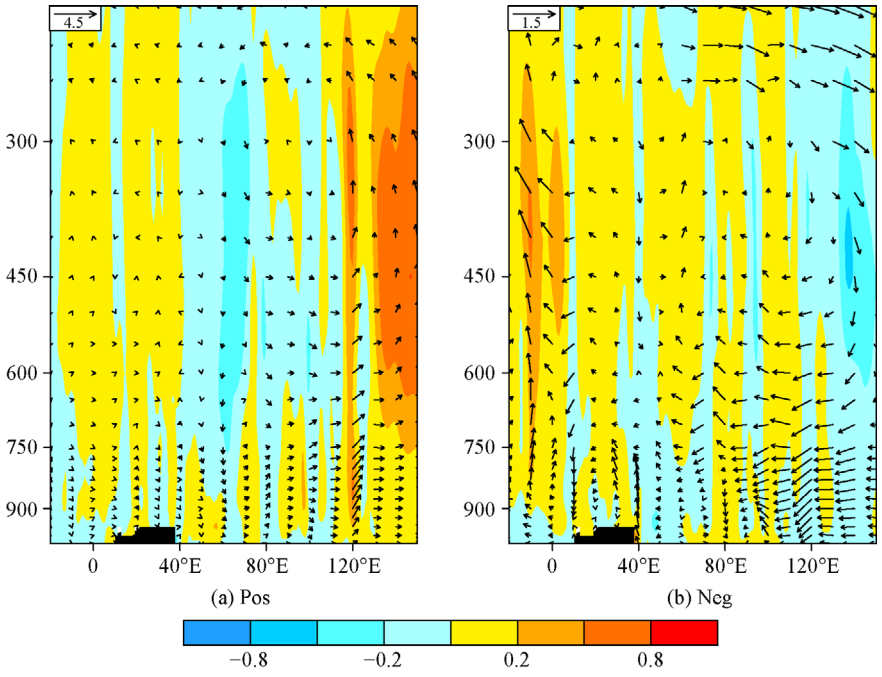

Fig. 17 Vertical–zonal profiles of anomalous u–w winds (vectors) and the Q_1 (shaded) in summer at 0°–20°N. Pos represents $QI \geqslant 1$; Neg represents $QI < 1$; and black shading denotes the topography.

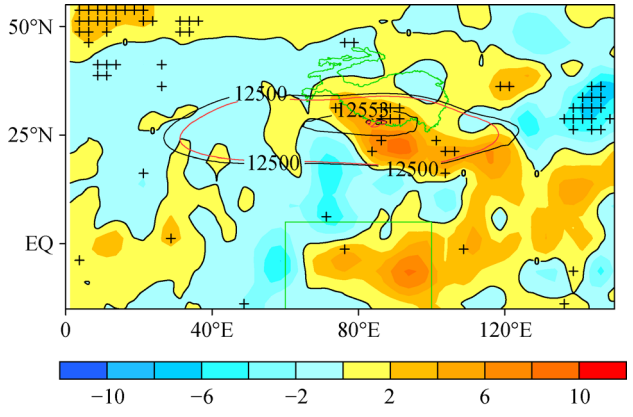

Fig. 18 Difference in summer precipitation in the Asian monsoon region between positive and negative QI (units: mm/day; plus signs indicate areas passing the 95% significance test; and black line and red line (geopotential ⩾ 12500 gpm) represents the SAH area of $QI \geqslant 1$ and $QI < 1$ respectively; and black line and red line (geopotential ⩾ 12553 gpm) represents the SAH center of $QI \geqslant 1$ and $QI < 1$ respectively).

temperature over the BOB. When QI is abnormally low, the situation is almost the reverse.

6 Summary and discussion

6.1 Summary

The present study defined a thermal contrast index (QI) based on the integral of the whole atmosphere of AHS to analyze the differences in the TP heat source and the TIO heat source. The SASM index (or MI) proposed by Xu and Chan (2002) was used to investigate the relationship between the QI and SASM. The conclusions are summarized as follows.

1) The seasonal changes of Q_1 in the TP and TIO regions are opposite, but they are both heat sources in summer, with the strongest thermal contrast. In summer, these two heat sources are mainly characterized by deep convection heating in the upper troposphere, which will strengthen the SAH and the upper-tropospheric warming center. The meridional thermal index (QI) between the TP and TIO and the SASM MI have a significantly positive correlation over the same period, and the two indexes' seasonal changes are basically the same, which both get to be the strongest in July. The positive correlation between the thermal contrast in the upper troposphere and the SASM is more significant.

2) Diagnostic and statistical analysis revealed that when the TP–TIO meridional thermal gradient increases (QI is abnormally large), the upper troposphere is warmer over Eurasia and the TIO is colder, resulting in the meridional temperature gradient and the baroclinicity of the troposphere increasing. Therefore, the low-level westerly airflow and the upper-level easterly airflow enhance, meaning the Walker circulation over the equatorial Indian Ocean is also enhanced and there is more precipitation over the SASM region. In years of abnormally low QI the situation is almost the reverse.

3) Based on the above analysis, and combined with

thermal wind theory and the T–Q_z relationship, the positive feedback mechanism underpinning the relationship between the TP–TIO thermal contrast and the SASM circulation was established. To sum up this mechanism, when the meridional thermal contrast is anomalous, the temperature gradient anomaly in the upper troposphere affects the baroclinicity of the atmosphere, resulting in anomalous monsoon circulation and eventually anomalous precipitation.

6.2 Discussion

This paper reveals a significant positive correlation between the thermal difference in the upper troposphere of the TP–TIO region and the SASM circulation, the results which can also be obtained using JRA-55 data. However, the *QI* and TI_{up} thermal contrast indices and the *MI* and WYI (Webster and Yang, 1992) SASM indices all show an increasing trend on the interdecadal scale during 1979–2019 in ERA5 data, while *QI* and TI_{up} show a decreasing trend according to JRA-55. This indicates some uncertainties in estimating the thermal contrast with reanalysis data, and the reason may stem from the resolution and assimilation methods related to the different reanalysis data sets. The next step in this research, therefore, will focus on the interdecadal variations of the thermal contrast at different levels of the atmosphere, as explored via numerical simulation experiments or CMIP6 data.

Acknowledgements This research is supported by the the Second Tibetan Plateau Scientific Expedition and Research (STEP) Program (No. 2019QZKK0105), the Strategic Priority Research Program of Chinese Academy of Sciences (No. XDA20060501) and the 2019 Non-funded Science and Technology Research Project of Zhanjiang (No. 20051817454-6338).

References

Chou C (2003). Land-sea heating contrast in an idealized Asian summer monsoon. Clim Dyn, 21(1): 11–25

Dai A G, Li H M, Sun Y, Hong L C, Ho L, Chou C, Zhou T J (2013). The relative roles of upper and lower tropospheric thermal contrasts and tropical influences in driving Asian summer monsoons. J Geophys Res, 118(13): 7024–7045

Duan A M, Wu G X (2005). Role of the Tibetan Plateau thermal forcing in the summer climate patterns over subtropical Asia. Clim Dyn, 24 (7–8): 793–807

Fu C, Fletcher J O (1985). The relationship between Tibet-tropical ocean thermal contrast and interannual variability of Indian monsoon rainfall. J Appl Meteorol, 24(8): 841–847

Goswami B N, Krishnamurthy V, Annmalai H (1999). A broad-scale circulation index for the interannual variability of the Indian summer monsoon. Q J R Meteorol Soc, 125(554): 611–633

Guan Z Y, Xu J J, Guo P W, Wang C (1997). The structure and variations of Asian summer monsoon reveled by barotropic and baroclinic modes the baroclinic mode analysis. Acta Meteorol Sin, 55(02): 19–26 (in Chinese)

Guan Z (2000). The variations of Asian monsoon as revealed by the variations of kinetic energy of barotropic/baroclinic modes of the wind field. Transactions of Atmospheric Sciences, 23(03): 313–322 (in Chinese)

Hansen J, Ruedy R, Sato M, Lo K (2010). Global surface temperature change. Rev Geophys, 48(4): RG4004

He H Y, Sui C H, Jian M Q, Wen Z P, Lan G (2003). The evolution of tropospheric temperature field and its relationship with the onset of Asian summer monsoon. J Meteorol Soc Jpn, 81(5): 1201–1223

He Y L, Huang J P, Ji M J (2014). Impact of land–sea thermal contrast on interdecadal variation in circulation and blocking. Clim Dyn, 43(12): 3267–3279

Hersbach H, Bell B, Berrisford P, Hirahara S, Horányi A, Muñoz-Sabater J, Nicolas J, Peubey C, Radu R, Schepers D, Simmons A, Soci C, Abdalla S, Abellan X, Balsamo G, Bechtold P, Biavati G, Bidlot J, Bonavita M, De Chiara G, Dahlgren P, Dee D, Diamantakis M, Dragani R, Flemming J, Forbes R, Fuentes M, Geer A, Haimberger L, Healy S, Hogan R J, Hólm E, Janisková M, Keeley S, Laloyaux P, Lopez P, Lupu C, Radnoti G, de Rosnay P, Rozum I, Vamborg F, Villaume S, Thépaut J (2020). The ERA5 global reanalysis. Q J R Meteorol Soc, 146(730): 1999–2049.

Huang J Y, Li Q X (2015). Methods for Statistical Analysis of Meteorological Data. Beijing: Meteorology Press (in Chinese)

Holton J R, Hakim G J (2004). An Introduction to Dynamic Meteorology. Burlington: Elsevier Acad

Kripalani R H, Kulkarni A, Sabade S S, Khandekar M L (2003). Indian Monsoon variability in a global warming scenario. Nat Hazards, 29 (2): 189–206

Li C F, Yanai M (1996). The onset and interannual variability of the Asian summer monsoon in relation to land-sea thermal contrast. J Clim, 9(2): 358–375

Li J P, Zeng Q C (2002). A unified monsoon index. Geophys Res Lett, 29(8): 115–1–115–4.

Liebmann B,Smith C A (1996). Description of a complete (interpolated)— outgoing longwave radiation dataset. Bull Amer Meteor Soc, 77(6): 1275–1277

Liu X, Wu G X, Liu Y M, Liu P (2002). Diabatic heating over the Tibetan Plateau and seasonal variastions of the Asian Circulation and summer monsoon. Chin J Atmos Sci, 6: 781–793 (in Chinese)

Liu X, Yanai M (2001). Relationship between the Indian monsoon rainfall and the tropospheric temperature over the Eurasia Continent. Q J R Meteorol Soc, 127(573): 909–937

Liu Y M, Wu G X, Hong J L, Dong B W, Duan A M, Bao Q, Zhou T J (2012). Revisiting Asian monsoon formation and change associated with Tibetan Plateau forcing: I. Formation. Clim Dyn, 39(5): 1169–1181

Liu Y M, Wu G X, Liu H, Liu P (1999). The effect of spatially nonuniform heating on the formation and variation of subtropical high part III: condensation heating and south Asia high and western Pacific. Acta Meteorol Sin, 57(5): 525–538 (in Chinese)

Luo X Q, Xu J J (2019). Estimate of atmospheric heat source over Tibetan Plateau and its uncertainties. Climate Change Research, 15 (1): 33–40 (in Chinese)

Luo X Q, Xu J J, Li K (2019). A review of atmospheric heat sources over the Tibetan Plateau. J Guangdong Ocean Univ, 39(06): 130–136 (in Chinese)

Naveendrakumar G, Vithanage M, Kwon H H, Chandrasekara S S K, Iqbal M C, Pathmarajah S, Fernando W C D K, Obeysekera J (2019). South Asian perspective on temperature and rainfall extremes: a review. Atmos Res, 225: 110–120

Parthasarathy B, Kumar K R, Kothawale D R (1992). Indian summer monsoon rainfall indices: 1871–1990. Meteorological Magazine, 121 (1441): 174–186

Roxy M K, Ritika K, Terray P, Murtugudde R, Ashok K, Goswami B N (2015). Drying of Indian subcontinent by rapid Indian Ocean warming and a weakening land-sea thermal gradient. Nat Commun, 6 (1): 7423

Sontakke N A, Pant G B, Singh N (1993). Construction of all-India summer monsoon rainfall series for the period 1844–1991. J Clim, 6 (9): 1807–1811

Sun X R, Chen L X, He J H (2002). Index of the sea thermal difference and its relation to interannual variation of summer circulation and rainfall over East Asian. Acta Meteorol Sin, 60(02): 164–172 (in Chinese)

Sun Y, Ding Y H, Dai A G (2010). Changing links between South Asian summer monsoon circulation and tropospheric land-sea thermal contrasts under a warming scenario, Geophys Res Lett, 37(2):195–205

Turner A G, Annamalai H (2012). Climate change and the South Asian summer monsoon. Nat Clim Chang, 2(8): 587–595

Tu H W, Tian H Y, Xu X, Zhang R (2020). Influence of the south-north displacement of South Asia High on the distribution of atmospheric composition in the upper troposphere-lower stratosphere over the Asian Monsoon Region. Plateau Meteorol, 39(2): 333–346

Wang B, Fan Z (1999). Choice of South Asian summer monsoon indices. Bull Am Meteorol Soc, 80(4): 629–638

Wang B, Liu J, Kim H J, Webster P J, Yim S Y, Xiang B (2013). Northern Hemisphere summer monsoon intensified by mega-El Nino/southern oscillation and Atlantic multidecadal oscillation. Proc Natl Acad Sci USA, 110(14): 5347–5352

Wang P X, Wang B, Cheng H, Fasullo J, Guo Z T, Kiefer T, Liu Z Y (2017). The global monsoon across time scales: mechanisms and outstanding issues. Earth Sci Rev, 174: 84–121

Wang Y N, Zhang B, Chen L X, He J H, Li W, Chen H (2008). Relationship between the atmospheric heat source over Tibetan Plateau and the heat source and general circulation over East Asia. Sci Bull (Beijing), 53(21): 3387–3394

Webster P J, Magaña V O, Palmer T N, Shukla J, Tomas R A, Yanai M, Yasunari T (1998). Monsoons: processes, predictability, and the prospects for prediction. J Geophys Res D Atmospheres, 103(C7): 14451–14510

Webster P J, Yang S (1992). Monsoon and Enso: selectively interactive systems. Q J R Meteorol Soc, 118(507): 877–926

Wei W (2015). The interannual shift of the South Asia High and its relation with the Asian summer monsoon. Dissertation for the Doctoral Degree. Beijing: Chinese Academy of Meteorological Sciences (in Chinese)

Wu G X, Duan A M, Liu Y M, Yang J H, Liu B Q, Ren S L, Zhang Y N, Wang T M, Liang X Y, Guan Y(2013). Recent advances in the study on the dynamics of the Asian summer monsoon onset. Chin J Atmos Sci, 37(2): 211–228 (in Chinese)

Wu G X, Bian H, Liu Y M, Bao Q, Ren R C, Liu B Q (2016). Recent progresses on dynamics of the Tibetan Plateau and Asian summer monsoon. Chin J Atmos Sci, 40(1): 22–32 (in Chinese)

Wu G, Liu Y (2003). Summertime quadruplet heating pattern in the subtropics and the associated atmospheric circulation. Geophys Res Lett, 30(5): 5–1

Wu G, Liu Y, He B, Bao Q, Duan A, Jin F F (2012). Thermal controls on the Asian summer monsoon. Sci Rep, 2(1): 404

Wu G X, Liu Y M, Liu X, Duan A M, Liang X Y(2005). How the heating over the Tibetan Plateau affects the Asian climate in summer. Chinese Journal of Atmospheric Sciences, 29(1):47–56 + 167–168 (in Chinese)

Xu J J, Chan J C L (2002). Relationship between the planetary—scale circulation over East Asia and the intensity of the South Asian Summer Monsoon. Geophys Res Lett, 29(18): 1866

Yanai M, Li C F, Song Z S (1992). Seasonal heating of the Tibetan Plateau and its effects on the evolution of the Asian summer monsoon. J Meteorol Soc Jpn, 70(1B): 319–351

Yanai M, Tomita T (1998). Seasonal and interannual variability of atmospheric heat sources and moisture sinks as determined from NCEP–NCAR reanalysis. J Clim, 11(3): 463–482

Yanai M, Wu G X (2006). Effects of the Tibetan plateau. In: The Asian Monsoon. Heidelberg: Springer, 513–549

You Q, Min J, Zhang W, Pepin N, Kang S (2015). Comparison of multiple datasets with gridded precipitation observations over the Tibetan Plateau. Clim Dyn, 45(3–4): 791–806

Zhang Y, Fan G, Hua W, Zhang Y, Wang B, Lai X (2017). Differences in atmospheric heat source between the Tibetan Plateau–South Asia region and the southern Indian Ocean and their impacts on the Indian summer monsoon outbreak. J Meteorol Res, 31(3): 540–554

Zhan R F, Li J P (2008). The effect of atmospheric heat source in the Tibetan Plateau and the tropical Northwest Pacific Ocean on the interdecadal variation of summer stratospheric-tropospheric water vapor exchange in Asia. Sci China Ser D Earth Sci, 38(8): 1028–1040 (in Chinese)

Zhao Y, Duan A M, Wu G X, Sun R Z (2019). Response of the Indian ocean to the Tibetan Plateau thermal forcing in late spring. J Clim, 32 (20): 6917–6938